Int. J. Solids Structures Vol. 19, No. 12, pp. 1027–1034, 1983
Printed in Great Britain.

0020-7683/83 $3.00 + .00
Pergamon Press Ltd.

STABILITY OF AN ELASTIC–PLASTIC ARCH MODEL UNDER MULTIPLE LOADS

M. J. MIKKOLA
Department of Civil Engineering, Helsinki University of Technology, Otaniemi, Finland

and

R. H. PLAUT and H.-H. SHEU
Department of Civil Engineering, Virginia Polytechnic Institute and State University, Blacksburg, VA 24061, U.S.A.

(*Received* 27 *December* 1982; *in revised form* 25 *April* 1983)

Abstract—The behavior of an arch model which exhibits inelastic material behavior and pre-buckling deformations is investigated. A bilinear stress–strain relationship is assumed. Both symmetric and asymmetric loading conditions are considered, and attention is focused on critical loads for snap-through instability. With the use of arbitrary ratios of independent loads, interaction curves are determined. It is seen that the magnitude of the yield force has a significant effect on the form of these curves.

INTRODUCTION

A simple model of an inelastic arch was introduced by Augusti[1] and examined further by Batterman[2]. The model, shown in Fig. 1, consisted of four weightless bars, three hinges, and two deformable cells. The cell elements obeyed a bilinear stress–strain relationship. Equal loads were applied ($q_1 = q_2$), and it was assumed that the bars experienced no rotations until the central two bars, acting like a column, began to buckle. The results were compared to those of Shanley[3] for an elastic–plastic column. Batterman also analyzed the model with an initial vertical deflection of the central hinge.

Other papers dealing with inelastic arches and arch-type structures include Refs.[4–10].

The model investigated in the present paper is similar to that treated by Augusti[1] and Batterman[2]. However, prebuckling deformations are included in the analysis, to give a more accurate picture of the behavior of actual arches. Therefore instability does not involve

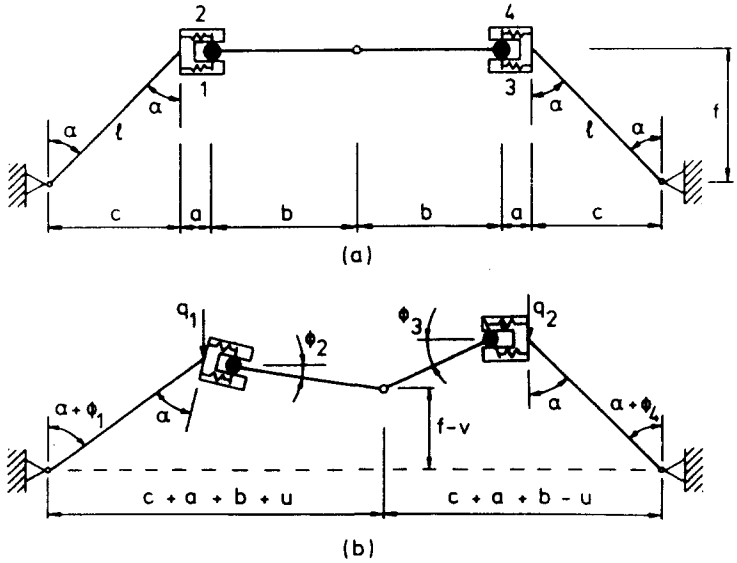

Fig. 1. Geometry of arch model.

bifurcation from a trivial equilibrium state, but requires the determination of the load-deflection equilibrium path from the onset of loading. Also, the loading is not restricted to be symmetric. Arbitrary combinations of q_1 and q_2 are considered, and it is shown that the model may be much weaker under asymmetric loading conditions. Interaction curves of critical loads are obtained in order to demonstrate the effect of the load ratio q_1/q_2 on the stability of the structure. The form of the interaction curve depends greatly on the magnitude of the yield force.

DESCRIPTION OF MODEL

The configuration of the unloaded model is depicted in Fig. 1(a). The outer bars have length l and angle α with the vertical. The inner bars are horizontal at the height f above the supports and have length b. The cell elements have undeformed length a. In Fig. 1(b), the equilibrium configuration is shown when vertical loads q_1 and q_2 act at the inner ends of the outer bars. The rotations of the bars are denoted ϕ_i, where ϕ_1 and ϕ_2 are positive clockwise while ϕ_3 and ϕ_4 are positive counter-clockwise. The horizontal and vertical deflections of the central hinge are denoted u and v, respectively, with u positive to the right and v positive downward.

The model has four degrees of freedom, and the quantities ϕ_1, ϕ_4, u and v will be used as the generalized coordinates. The four rotations ϕ_i are not a suitable choice, because they do not always define the configuration uniquely. For example, if $\phi_1 = \phi_4 = 0$ and $\phi_2 = \phi_3$, the horizontal position of the central hinge is not uniquely determined.

The cell elements are numbered 1, 2, 3 and 4, as shown in Fig. 1(a), and their lengths are denoted a_1, a_2, a_3, and a_4, respectively, with $a_i = a$ when $q_1 = q_2 = 0$. In Fig. 2, the geometry of the left cell is illustrated for undeformed and deformed conditions. The distance between the cell elements is d. The inner bar is connected to a circular pin which is allowed to slide and rotate in a central channel between the elements. A rigid rod is connected to the pin, perpendicular to the inner bar. The cell elements are modeled as elastic-plastic springs, and when the pin slides or rotates (or both), each spring exerts a compressive or tensile force on the rod. The springs are confined to certain channels, and their points of application on the rod vary as the pin rotates.† (Due to this, the spring forces are nonconservative. Therefore, dynamic (flutter) instability is a possibility; however, it does not occur in the model treated here, and only a static analysis is described.) This cell was devised in order to obtain rotations of the bars as soon as the loads are applied, without introducing additional degrees of freedom.

The force acting on cell element i is denoted r_i and is positive in compression. A bilinear relationship is used, representing an elastic, linearly strain hardening material, as depicted in Fig. 3. The yield force r_0, the elastic spring constant K, and the plastic spring constant K_T are assumed to be the same for each cell element. To account for the Bauschinger effect, the assumption of kinematic hardening is employed.

FORMULATION OF EQUILIBRIUM EQUATIONS

From Fig. 1(a), one has

$$c = l \sin \alpha, f = l \cos \alpha. \tag{1}$$

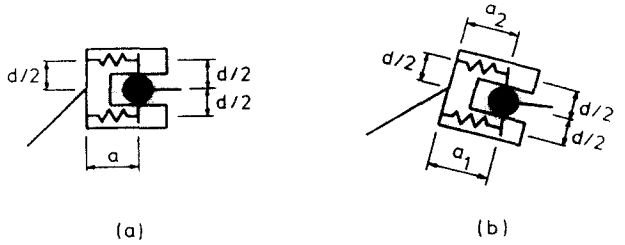

Fig. 2. Geometry of cell.

†If the springs were attached to the rods, the behavior of the model would probably be similar as long as the rotations of the cells remain small.

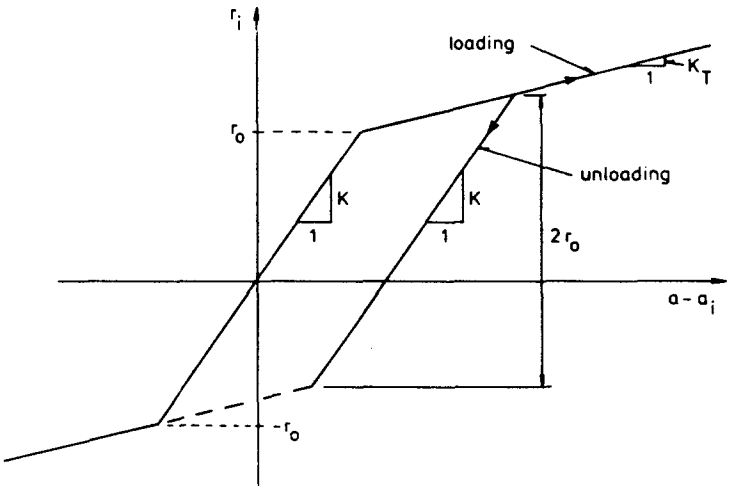

Fig. 3. Force-displacement relationship.

From Fig. 1(b), considering the horizontal distance from the left support to the central hinge, one can show that

$$c + a + b + u = l \sin(\alpha + \phi_1) + (d/2) \cos \phi_1 \tan(\phi_2 - \phi_1) + a_1 \cos \phi_1 + b \cos \phi_2 \tag{2}$$

if one passes through cell element 1. If one passes through cell element 2 and compares the result with (2), one obtains

$$a_2 = a_1 + d \tan(\phi_2 - \phi_1). \tag{3}$$

A similar procedure on the right side of the model yields

$$c + a + b - u = l \sin(\alpha + \phi_4) + (d/2) \cos \phi_4 \tan(\phi_3 - \phi_4) + a_3 \cos \phi_4 + b \cos \phi_3 \tag{4}$$

and

$$a_4 = a_3 + d \tan(\phi_3 - \phi_4). \tag{5}$$

From the vertical distance from the left support to the central hinge, passing through cell element 1, one gets

$$f - v = l \cos(\alpha + \phi_1) + (d/2) \sin \phi_1 \tan(\phi_1 - \phi_2) - a_1 \sin \phi_1 - b \sin \phi_2. \tag{6}$$

Similarly, passing through cell 3 on the right side,

$$f - v = l \cos(\alpha + \phi_4) + (d/2) \sin \phi_4 \tan(\phi_4 - \phi_3) - a_3 \sin \phi_4 - b \sin \phi_3. \tag{7}$$

From (1)–(7), one can obtain the equations

$$b \sin(\phi_2 - \phi_1) = v \cos \phi_1 - (c + a + b + u) \sin \sin \phi_1 + (1 - \cos \phi_1) f \tag{8}$$

and

$$b \sin(\phi_3 - \phi_4) = v \cos \phi_4 - (c + a + b - u) \sin \phi_4 + (1 - \cos \phi_4) f. \tag{9}$$

For given values of the independent variables ϕ_1, ϕ_4, u, and v, one can determine ϕ_2 from (8), ϕ_3 from (9), a_1 from (2), a_2 from (3), a_3 from (4), and a_4 from (5).

The spring forces r_i are obtained from the relationship depicted in Fig. 3. In order to derive

the equilibrium equations for the model, consider the free body diagrams of the two bars on the left side of the model shown in Fig. 4. The quantity s_L represents the force perpendicular to the cell elements which is transmitted between the outer and inner bars through the left cell, acting at the left end of the inner bar. Equilibrium of moments about the support in Fig. 4(a) yields

$$q_1 l \sin(\alpha + \phi_1) = [c + (a_1 + a_2)/2]s_L + (r_1 + r_2)f + (r_2 - r_1)d/2. \tag{10}$$

The corresponding equation on the right side of the model is given by

$$q_2 l \sin(\alpha + \phi_4) = [c + (a_3 + a_4)/2]s_R + (r_3 + r_4)f + (r_4 - r_3)d/2, \tag{11}$$

where s_R is defined in a similar manner as s_L. Equilibrium of moments about the hinge in Fig. 4(b) yields

$$s_L b \cos(\phi_2 - \phi_1) = (r_1 + r_2)b \sin(\phi_2 - \phi_1) + (r_2 - r_1)d/2. \tag{12}$$

Similarly, from the right side,

$$s_R b \cos(\phi_3 - \phi_4) = (r_3 + r_4)b \sin(\phi_3 - \phi_4) + (r_4 - r_3)d/2. \tag{13}$$

Finally, if one considers a free body diagram of the two inner bars together and takes equilibrium of horizontal and vertical force components, one gets

$$(r_1 + r_2)\cos\phi_1 - s_L \sin\phi_1 - (r_3 + r_4)\cos\phi_4 + s_R \sin\phi_4 = 0, \tag{14}$$

and

$$(r_1 + r_2)\sin\phi_1 + s_L \cos\phi_1 + (r_3 + r_4)\sin\phi_4 + s_R \cos\phi_4 = 0. \tag{15}$$

In the analysis, s_L is obtained from (12) and s_R from (13). Then, after using (8), (9), (2), . . . , (5), and the stress–strain relationship as described previously, the equilibrium equations (10), (11), (14) and (15), involving ϕ_1, ϕ_4, u, v, q_1 and q_2, are solved numerically.

The following dimensionless quantities are utilized in the computations and the presentation of the results:

$$A = \frac{a}{f},\ A_i = \frac{a_i}{f},\ B = \frac{b}{f},$$
$$C = \frac{c}{f},\ D = \frac{d}{f},\ U = \frac{u}{f},\ V = \frac{v}{f},$$
$$R_0 = \frac{2bcr_0}{Kfd^2},\ R_i = \frac{2bcr_i}{Kfd^2},\ Q_i = \frac{2bcq_i}{Kfd^2},\ \lambda_T = \frac{K_T}{K}, \tag{16}$$

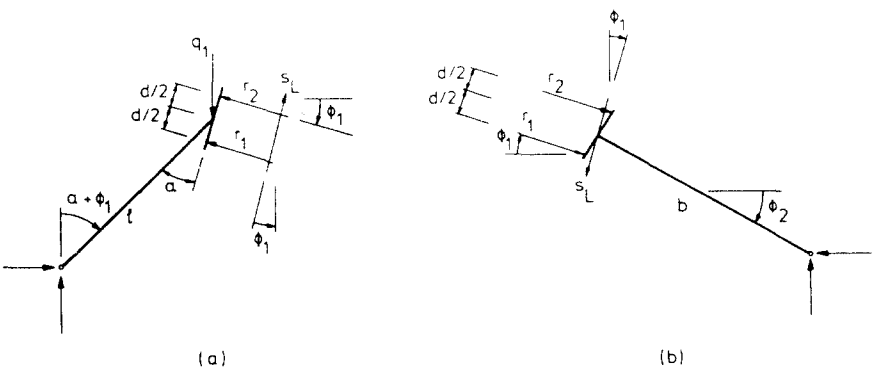

Fig. 4. Free body diagrams of left outer and inner bars.

where $i = 1, 2, 3, 4$ and $j = 1, 2$. In the numerical examples, the following geometrical parameters are used:

$$A = 0.1, B = 1, C = 1, D = 0.1. \tag{17}$$

Then $\alpha = \pi/4$ and the height-to-span ratio is 1/4.2.

SYMMETRIC CASE

In this section, assume that the loading and deflection are symmetric, so that

$$Q_1 = Q_2 \equiv Q, \phi_3 = \phi_2, \phi_4 = \phi_1, U = 0,$$
$$A_3 = A_1, A_4 = A_2, R_3 = R_1, R_4 = R_2. \tag{18}$$

From equilibrium considerations, there is no vertical force at the hinge in Fig. 4(b), and it follows from (12) and equilibrium of vertical force components that

$$(r_1 + r_2)b \sin \phi_2 = (r_1 - r_2)(d/2) \cos \phi_1. \tag{19}$$

In dimensionless terms, (8) becomes

$$B \sin (\phi_2 - \phi_1) = 1 + (V - 1) \cos \phi_1 - (C + A + B) \sin \phi_1. \tag{20}$$

With the use of (2), (3), (10), (12) and (19), one can obtain

$$(C \cos \phi_1 + \sin \phi_1)Q = (R_2 - R_1)(D/2) + (R_1 + R_2)$$
$$- (R_1 + R_2)(C + A + B - \sin \phi_1 - B \cos \phi_2) \sin \phi_1/\cos^2 \phi_1. \tag{21}$$

Finally, (19)–(21) can be combined to yield

$$(C \cos \phi_1 + \sin \phi_1)Q \cos \phi_1 + (V - 1)(R_1 + R_2) = 0. \tag{22}$$

The coordinate ϕ_2 can be determined from (20), and then (21) and (22) are the governing equilibrium equations in ϕ_1 and V.

On the equilibrium path, starting from the unloaded configuration, ϕ_1 increases monotonically. The load Q, however, increases and then decreases. Therefore, in the iterative solution procedure, ϕ_1 is incremented and ϕ_2, V, and Q are computed numerically from (20) to (22).

First, assume R_0 is sufficiently large so that the behavior remains elastic until after instability occurs. The resulting equilibrium path (Q vs V) is depicted in Fig. 5. It possesses a

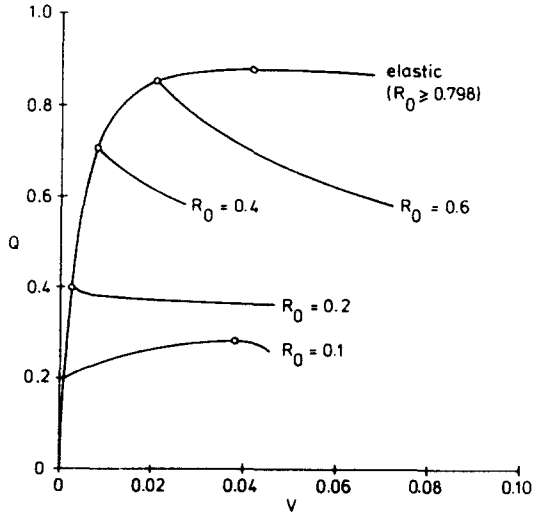

Fig. 5. Equilibrium paths for symmetric case ($\lambda_T = 0.25$, various R_0).

limit point (maximum point) at $Q = 0.880$ and $V = 0.040$ (critical points are designated by circles). For this equilibrium state, $\phi_1 = 0.003$, $\phi_2 = 0.037$, $R_1 = 0.798$, and $R_2 = 0.121$. If Q is raised beyond this critical value, the arch will snap to an inverted configuration for which $V = 2.303$, $\phi_1 = 1.201$, and $\phi_2 = 0.692$.

Some other geometrical configurations of the model were considered in this elastic analysis, in order to see the effect on the critical load. In one case, a, c, d and f were fixed, according to (17), and b was varied from $0.5f$ to $10f$ (see Fig. 1a). In the other, b, d and f were fixed, and b and c were varied together from $b = c = 0.1f$ to $b = c = 2f$. For all these cases, the critical value of the dimensionless load Q did not change by more than 1% from $Q = 0.880$. Of course, the dimensional critical load decreases as b and c are increased, according to (16).

For the elastic–plastic behavior shown in Fig. 3, the critical load is still given by $Q = 0.880$ if $R_0 \geq 0.798$, since then the spring forces do not reach the yield force before snap-through occurs. Equilibrium paths for $\lambda_T = 0.25$ and $R_0 = 0.6$, 0.4, 0.2, and 0.1 are shown in Fig. 5. In the first three of these cases, the path begins to have a decreasing slope as soon as $R_1 = R_0$, i.e. when the forces in cell elements 1 and 3 reach the yield force.† The corresponding value of Q is then the critical load. For $R_0 = 0.1$, however, the path continues to have a positive slope after springs 1 and 3 become plastic, until it reaches a limit point.

GENERAL CASE

Arbitrary combined loads Q_1 and Q_2 are considered now. The loads are increased proportionally. In the loading plane Q_1 versus Q_2 (Figs. 6 and 7) this corresponds to moving along a ray $Q_2 = \gamma Q_1$ from the origin. For the numerical procedure, γ is fixed at some value between 0 and 1, ϕ_1 is incremented, and ϕ_2, U, V, and Q_1 are determined from the dimensionless versions of (10), (11), (14) and (15). The symmetric case corresponds to the bisecting ray $\gamma = 1$, while $\gamma = 0$ gives the single load case along the Q_1 axis. Results for $\gamma > 1$ are obtained by symmetry.

Critical loads are computed for a number of rays, and the locus of critical load combinations forms an interaction curve (stability boundary) in the loading plane. Results are presented for the elastic case and for $\lambda_T = 0.25$ with various values of the yield force R_0.

The interaction curve in Fig. 6 for the elastic case is slightly convex toward the origin except near the ray $\gamma = 1$. For the equilibrium configurations corresponding to points on this curve (i.e. at the verge of snap-through), with $0 \leq \gamma \leq 1$, R_1 is tensile if $0 \leq \gamma < 0.833$ and compressive if

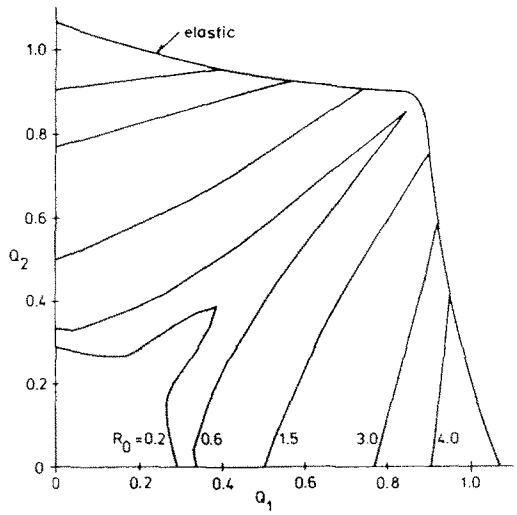

Fig. 6. Interaction curves ($\lambda_T = 0.25$, various R_0).

†This abrupt change of slope is due to the slope change from K to K_T in Fig. 3, and is not associated with bifurcation. In this section, the assumption $U = 0$ in (18) essentially prohibits the occurrence of bifurcation instability. When this assumption is dropped in the following section, it still turns out that bifurcation does not occur, for symmetric or asymmetric loading, if the geometrical parameters are given by (17).

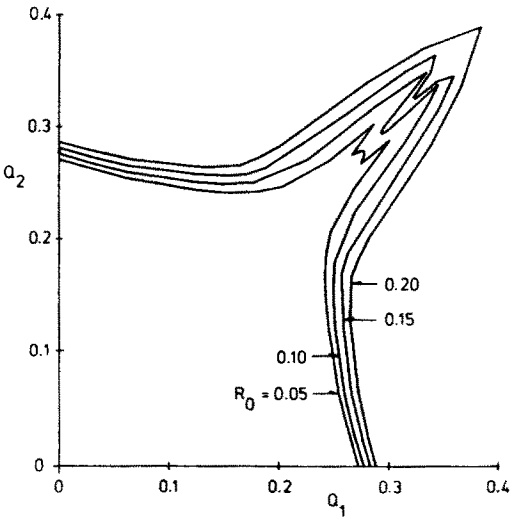

Fig. 7. Interaction curves ($\lambda_T = 0.25$, various R_0).

$0.833 < \gamma \leq 1$, R_2 and R_3 are always compressive, and R_4 is tensile if $0 \leq \gamma < 0.989$ and compressive if $0.989 < \gamma \leq 1$. Also, R_3 always has the highest magnitude.

Elastic interaction curves were also determined for $B = 2$ and $B = 4$ in (17). They are very similar to the elastic curve in Fig. 6 and both have $Q_1 = 0.884$ for $\gamma = 1$ and $Q_1 = 0.96$ for $\gamma = 0$.

In the elastic-plastic case with $\lambda_T = 0.25$, the elastic curve still governs for all loading rays if $R_0 \geq 6.949$. If $0.789 < R_0 < 6.949$, the elastic curve gives the critical loads for a range of γ values about $\gamma = 1$. On the other rays, one or more of the springs become plastic and the critical load is less than that for the elastic case. This situation is seen in Fig. 6 when $R_0 = 4.0$, 3.0, and 1.5, with part of each stability boundary governed by elastic behavior and part by plasticity. Finally, if $0 < R_0 < 0.789$, plasticity governs the entire interaction curve. The cases $R_0 = 0.6$ and 0.2 in this last category are shown in Fig. 6.

In Fig. 7, the interaction curve for $R_0 = 0.2$ is plotted again, along with those for $R_0 = 0.15$, 0.10 and 0.05. The behavior near the ray $\gamma = 1$ is quite irregular. For the symmetric case $\gamma = 1$, recall that the critical load corresponds to the onset of plastic behavior if $0.175 \leq R_0 < 0.798$. The interaction curves for $R_0 = 0.2$ and 0.6, which fall in this range, show a smooth decrease in critical load as γ decreases from unity (i.e. as the loading becomes asymmetric). However, if $R_0 = 0.15$, 0.10 or 0.05, when the symmetric critical load corresponds to a limit point, the model is stronger for some slightly asymmetric loading conditions than it is for symmetric loading. This irregular behavior only exists in a small neighborhood of the ray $\gamma = 1$.

CONCLUSIONS

The snap-through instability of a four-degree-of-freedom arch model with elastic-plastic deformable cells has been investigated. A bilinear force-displacement relation has been assumed for the cell elements. Two loads, applied quasi-statically and proportionally, have been considered and pre-buckling deformations have been included in the analysis. By taking different ratios of the loads, interaction curves of critical load combinations have been constructed.

The case of symmetric loading has been examined first. The effect of the yield force is illustrated in Fig. 5. The critical load increases or remains constant if the yield force is increased, or if the ratio of the plastic spring constant to the elastic spring constant, K_T/K, is increased.

Interaction curves for the general case are presented in Figs. 6 and 7. The plastic spring constant is assumed to be one-fourth of the elastic spring constant and the dimensionless yield force R_0 is varied. The form of the interaction curve depends greatly on R_0. For sufficiently high R_0, none of the springs becomes plastic before snap-through and the elastic curve governs. The form of this curve is completely different from that when plasticity governs. For example,

when $R_0 = 0.6$ in Fig. 6, there is a sharp point in the curve at the symmetric ray and critical values for asymmetric loading may be much lower than those for symmetric loading. In other words, a critical load based on the symmetric case may be very misleading.

The type of behavior of the model depends on the yield force, the spring constant ratio and the load ratio. If the yield force is high enough, snap-through occurs elastically when the equilibrium path exhibits a limit point. In an intermediate range, snap-through occurs as soon as one of the springs becomes plastic. For sufficiently small values of the yield force, one or more springs behaves plastically and snap-through occurs either at a limit point (with zero slope) or at a point of discontinuous slope (from a positive to a negative value) when a spring becomes plastic or begins to unload. When one of the first two types of behavior governs, the interaction curves are not affected by a change in the loading process. If plastic flow occurs, however, the interaction curves would be different if the loads were not applied proportionally.

Some of the features of the behavior are due to the discontinuity of slope in the loading process in Fig. 3, and would be altered if the slope changed continuously[11]. In particular, most critical points on the equilibrium paths would be limit points. The only exception would occur if one or more springs were in the plastic range and would begin to unload at the onset of instability, since this would involve a discontinuous change of slope.

Acknowledgements—This research was supported by the U.S. National Science Foundation under grant CME-7920781. Helpful comments by Dr. V. Tvergaard on the original manuscript are gratefully acknowledged.

REFERENCES

1. G. Augusti, Buckling of inelastic arches: a simple model. *Meccanica* **3**, 102 (1968).
2. S. C. Batterman, Plastic stability of arches: reconsideration of a model. *Israel J. Tech.* **9**, 467 (1971).
3. F. R. Shanley, Inelastic column theory. *J. Aeronaut. Sci.* **14**, 261 (1947).
4. V. Franciosi, G. Augusti, and R. Sparacio, Collapse of arches under repeated loading. *J. Struct. Div., Proc. ASCE* **90**, 165 (1964).
5. J. A. Stricklin, P.-T. Hsu and T. H. H. Pian, Large elastic, plastic, and creep deflections of curved beams and axisymmetric shells. *AIAA J.* **2**, 1613 (1964).
6. L. H. N. Lee and L. M. Murphy, Inelastic buckling of shallow arches. *J. Engng Mech. Div., Proc. ASCE* **94**, 225 (1968).
7. N. C. Huang and W. T. Tsai, Dynamic snap-through of an elastic-plastic simple shallow truss. *Int. J. Solids Structures* **5**, 737 (1969).
8. M. Mikkola and P. Timonen, Large deflections of elastic-plastic circular arches. In *Proc. II. Nordiske forskningsdager for stålkonstruksjoner*, Oslo, 20–22, Aug. 1973.
9. S. Kuranishi, Load carrying capacity of fixed arches. In *Stability of Structures Under Static and Dynamic Loads*, p. 609. ASCE Publications, New York (1977).
10. Z. Waszczyszyn, Numerical analysis of nonlinear structural instability. In *Stability in the Mechanics of Continua* (Edited by F. H. Schroeder). Springer-Verlag, Berlin (1982).
11. M. J. Sewell, A survey of plastic buckling. In *Stability* (Edited by H. Leipholz), pp. 85–197. University of Waterloo, Ontario (1972).